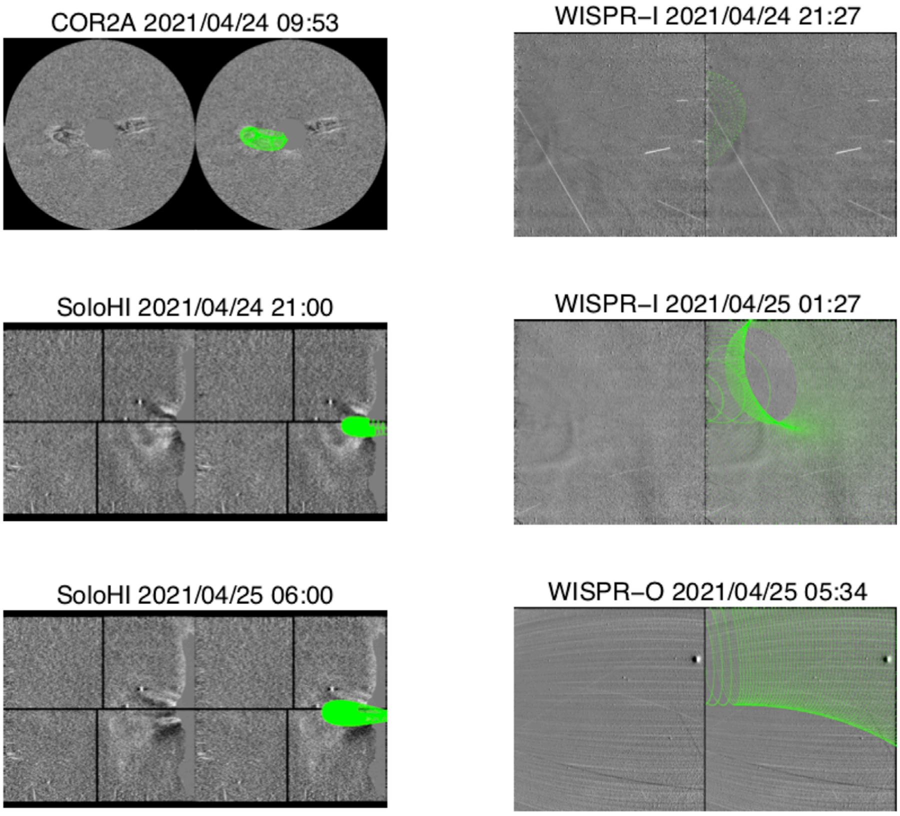


FIGURE 12
Example frames with (*right*) and without (*left*) the GCS mesh overlay from COR2, SoloHI, and WISPR-I and WISPR-O. The discrepancies between the GCS model and the observed features in the WISPR frames are due to the Thomson scattering effects.

several consecutive loop structures that continue to be observed after 2021 April 25, 12:00 UT.

Similarly, in WISPR-O, a number of separate distinct outflows are visible throughout 2021 April 25, as seen in Figure 11. This type of repeated outflow has not been seen before or after this event. We believe this is due to a combination of the spacecraft flying through the CME and the different distinct blobs seen in Figure 7F.

## 4.4 GCS reconstruction

The determined GCS structure (details of the model described in Section 2) is displayed in Figure 12. This structure was determined largely from the COR2 observations, making the geometry more uncertain given the single viewpoint. Later observations from WISPR and SoloHI, while not overlapping with COR2, were used to determine if this GCS structure was plausible.

The parameters of the model are listed in Table 2. Given the relatively faint CME observations and assuming low values of the width and aspect ratio (which controls the minor axis cross-section), we found that the CME nose is almost directly pointed at the PSP spacecraft.

COR2 and SoloHI were optimally positioned to observe the event. However, because the field of views did not overlap and had similar lines of sight, a true multi-viewpoint triangulation was not possible, and the reconstruction should be considered to have significant uncertainties. The SoloHI observations are further limited by the low resolution and cadence of the images due to the larger radial distance of the spacecraft. The WISPR data overlap with the SoloHI data at a much better resolution and cadence, but given that the derived GCS direction is pointing toward the PSP spacecraft, much of the CME front is likely unable to be resolved due to the poor Thompson scattering angle.

**TABLE 2 GCS parameters determined to best recreate the CME. The longitude and latitude have been converted into HEE coordinates for the sake of comparison to Table 1.**

| Lon(°) | Lat(°) | Tilt(°) | Aspect Ratio | Half Angle(°) |
|---|---|---|---|---|
| 162.9 | −5.08 | 13.98 | 0.125 | 20.12 |

It should be noted that the different outflows observed, especially the two apparent flux-rope-like structures seen through Figure 7C, make it challenging to directly and confidently link the *in situ* data to what is imaged remotely. By fitting the GCS to the clearest observed flux-rope seen in COR2, we have produced a plausible geometric and kinematic structure that seems to match the various observations. We do acknowledge the possibility that another structure, such as that seen in front of the structure, fits with the GCS model in Figure 7C and could have been oriented toward PSP and produced the resulting *in situ* signatures. Regardless, the kinematics of the

GCS blob should represent a useful velocity for the various related outflows seen in the imaging.

## 5 Discussion

To relate features observed in FSI and Metis, COR2, and PSP, we constructed a height–time plot (Figure 13) that combines the FSI and COR2 data, with overlays from measured or extrapolated positions of the eruptions as observed in other instruments. The plot shows the average over a radial cut through the images along the primary propagation direction of the eruption, between about 108° and 122° in the heliocentric radial coordinate system (where 0° is at the Sun's north pole and 90° points due east).

Above 4 $R_\odot$, we use COR2 observations to track the motion of the eruption, interpolated to match the spatial and temporal resolution of the FSI observations, and corrected to match the line of sight based on the known spacecraft locations and our 3D reconstruction (see Section 4.1). Note that the timing error introduced by SolO and STEREO-A's different distances from the Sun is about 45 s, which is negligible compared to the uncertainty introduced by the observation cadence of COR2 and the assumptions underpinning the de-projection of the STEREO-A data to match SolO's perspective, and are, therefore, neglected in this plot.

To relate the multiple observations, reconstructions, and extrapolations of the eruption from different instruments to one another and to validate that each tracking method has indeed produced self-consistent results, in a simple, unified view, we overlay our measurements of the position of the eruption on the height–time plot, including FSI (*red* +), COR2 GCS reconstructions (*light blue* *), Metis (*orange* □), and backward extrapolations from PSP's position using the velocities measured *in situ* (*first* transient in *magenta* +, constant speed patch in *green* +, and the second transient in *indigo* +; these colors are selected to generally correspond to the colors of specific field lines in Figure 2 but must be lightened somewhat to be visible on the dark height–time image).

From the *in situ* observations, we analytically reconstruct the speed values from the PSP location back to 10–20 $R_\odot$. We track back three different patches of plasma: the *first* structure (vertical *magenta* dash line in Figure 3) that crossed PSP at 412 km $s^{-1}$, the *second* at a constant speed of 300 km $s^{-1}$ (delimit between the two vertical *green* dash lines), and the *third* structure at 310 km $s^{-1}$ (vertical *indigo* dash line).

We assume steady flows of adiabatic gas in each patch to solve the 1D spherical symmetric Bernoulli's equation (integrated momentum equation) and obtain their speeds at ten different distances between 10 and 20 $R_\odot$. We neglect gravity forces, assume a polytropic gas (Shi et al., 2022, in our case, $\gamma = 5/3$), and include the molecular weight $\mu$ to consider the $He^{2+}/H^{+}$ density ratio measured by SWEAP, to get the following:

$$v^2 = \left(\frac{2\gamma}{\gamma - 1}\right)\left(\frac{kT}{\mu m_H}\right)\left[1 - \left(\frac{v_0 r_0^2}{v r^2}\right)^{\gamma - 1}\right],$$

where $k$ is the Boltzmann constant, $m_H$ is the proton mass, $v_0$ and $r_0$ are the speed and radial distance near the Sun (in this case between 10 and 20 $R_\odot$), and $v$ and $r$ are the speed and radial distance at the PSP location, respectively. We reconstruct analytically the information of the structures back to the Sun by assuming constant speed motion (see Figure 13).

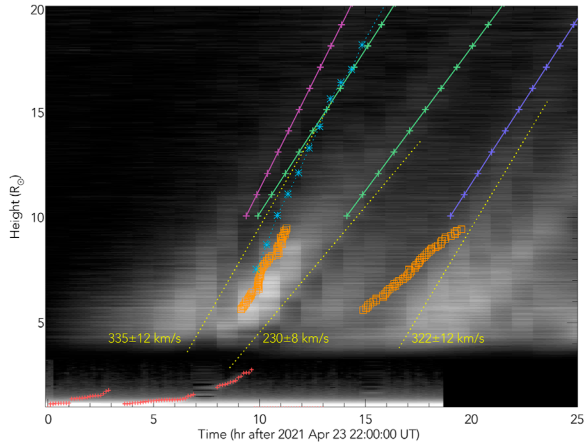


**FIGURE 13**
Composite FSI and Metis and COR2 height–time plot showing the relationships between erupting features tracked in EUI (*red* + symbols), COR2 GCS fits (*light blue* ⋆ symbols), Metis (*orange* □), and backward extrapolations from PSP *in situ* measurements of three different patches corresponding to those marked with vertical dash lines in Figure 3. The *first* transient with *magenta* +, the constant speed patch delimit between the lines marked with *green* +, and the *third* transient marked with *indigo* +. The dashed yellow lines and velocities are fit directly to features in the height–time plot.

In this case, we did not pursue running MHD numerical simulations (e.g., ENLIL (Odstrcil and Pizzo, 2009), PLUTO (Mignone et al., 2007; Mignone et al., 2012), and EUHFORIA (Pomoell and Poedts, 2018) numerical codes) by extrapolating the photospheric fields due to the difficulty of analyzing the event at its source region, observational limitations, and possible prediction of transit times to follow the eruption from the Sun to the PSP location with an analytical approach.

The analytical equations predict between 10 and 20 $R_\odot$: the passage of the *first* structure on 2021 April 24, 08:40 UT, propagating away from the Sun with a speed of 389 km $s^{-1}$, the constant speed structure on 2021 April 24, 10:00 to 18:00 UT, at 290 km $s^{-1}$, and the *third* transient on 2021 April 24, 23:00 UT, at 302 km $s^{-1}$.

Fitting the slopes of the two eruptions observed in the height–time plot, corresponding to the feature observed near the first sets of *orange* Metis points, we obtain a velocity of $335 \pm 12$ km $s^{-1}$. The second major eruption, around the second set of *orange* Metis points, has a velocity of $322 \pm 12$ km $s^{-1}$. A dark intermediate feature, corresponding to the third set of *red* points, is probably the trailing edge of the first eruption and has a slower speed, $230 \pm 8$ km $s^{-1}$.

The strong agreement between the different sets of observations suggests we are tracking the same features in all of our data. The velocities we measure from these height–time plots also agree well with the PSP-derived velocities, indicating that the propagation of the CME is not strongly influenced by interactions in interplanetary space.

Early in the first eruption, the prominence appears to follow the local magnetic field in the low corona, which is highly non-radial, and thus the radially plotted height–time diagram does not fully capture the prominence's trajectory or velocity. Outside of the FSI field of view, the eruption moves primarily radially, with essentially constant velocity.

By combining the analytical model with the connectivity derived from the MAS model, it is clear that, for much of the propagation of the eruption, the CME is propagating constantly along the open field lines connected to PSP because of the close proximity of the initial prominence to these field lines. While the magnetograms used in the MAS model for the area around the eruption are necessarily somewhat out of date because the eruption occurred on the backside of the Sun with respect to Earth, all of the remote-sensing data supports the notion of a simple propagation originating in the south and following open field lines northward toward the equator.

## 6 Conclusion

We reported the propagation of a complex prominence eruption that reached PSP on 2021 April 25 at 01:00 UT when the spacecraft was located at 46 $R_{\odot}$. To study the full evolution of the event, we combined multi-spacecraft remote-sensing observations with the *in situ* measurements onboard PSP. The structure, as sampled by SPC, was characterized as a low temperature and low-density transient with complex magnetic field configuration and a $He^{2+}/H^{+} > 8\%$ ratio indicating the presence of alpha particles identified from the clear secondary peak in the 1D reduced distribution functions moving at a velocity ranging between 550 and 650 km $s^{-1}$. Although the structure lacks a coherent magnetic field configuration, the rest of the characteristics observed are signatures common in magnetic clouds, particularly when related to prominences. We identified the complex prominence eruption as the source by tracking from the Sun to PSP location the propagation of the associated CME, which was only possible due to the nearly perfect quadrature of PSP and SolO.

We analyzed FSI, Metis, and COR2 images, tracked the structure evolution up to 20 $R_{\odot}$, and identified that the eruption occurred in two phases: a smaller outburst beginning in the more southerly part of a prominence and the substantial eruption originated from the more northerly part of the structure. Below 4 $R_{\odot}$, the set of remote-sensing observations showed that the structure is complex.

Above 20 $R_{\odot}$, the CME kinematics was modeled using the GCS reconstruction method over WISPR and COR2 coronagraph images and by modeling the background magnetic field using the MHD PSI/MAS model and backward analytic reconstruction starting from PSP *in situ* data. The strong agreement between the different sets of observations and models showed that the ICME propagated radially at a constant speed and that it was not strongly influenced by interactions in interplanetary space.

This work highlights the importance of studying the propagation of transients from a multi-spacecraft point of view, as their combination enables a better understanding of the phenomena by closing gaps between the sets, e.g., the distance ranges covered by the different instruments, the image dependence with the spacecraft location which also reverberates on the possibility to model the events from remote-sensing observations, and the limits of the current reconstruction models back to the Sun from *in situ* data. Particularly in this case, we were able to follow a complex structure that, during the first stages of propagation, it seems to be evolving non-radially before propagating at a constant rate. Moreover, the eruption conserves its plasma and magnetic properties up to 46 $R_{\odot}$.

## Data availability statement

PSP SWEAP and FIELDS data are publicly available and can be found at: https://cdaweb.gsfc.nasa.gov/. The SoloHI data will be accessible at https://solohi.nrl.navy.mil/so_data/L1/ while WISPR at https://wispr.nrl.navy.mil/data/rel/fits/L3/orbit08/ and SECCHI at https://stereo-ssc.nascom.nasa.gov/data/ins_data/secchi/L0/a. Metis data will become available through the Solar Orbiter Archive (SOAR) by the end of 2023. Data are in any case available from the instrument Principal Investigator, prof. Marco Romoli (marco.romoli@unifi.it) upon request. EUI data is available through the Solar Orbiter Archive (SOAR, https://soar.esac.esa.int/). Our MAS model results are all available online at www.predsci.com.

## Author contributions

TN, DS, PH, DB, VA, KK and MS contributed to conception, design of the study and writing of the first draft of the manuscript. TN carried out the PSP *in situ* data analysis and backward reconstruction models. MS performed the alpha ratio estimation and *in situ* data analysis. DS carried out height-time analysis for the near-sun observations and contributed to the characterization of the magnetic topology of the eruption's source region. PH performed analysis of the WISPR, SoloHI and COR2 images, including the GCS reconstruction of the CME on those data sets. DB contributed the EUI image processing and the visualization of the magnetic field lines. CV was the science planner and campaign leader for EUI that produced the EUI data analyzed in this paper. VA performed analysis of Metis data, including the determination of Metis height-time curves. PR and KR performed and worked the magnetic field simulations. FL and CS worked with the Metis observation plan that produced the Metis data analyzed in this paper. RS worked with the Metis observation plan and processed the resulting data analyzed in this paper. MU performed Metis UV data processing. All authors contributed to manuscript revision, and approved the submitted version. TN would like to thank Kristoff Paulson and Anthony Case for all their helpful discussions.

## Funding

Parker Solar Probe was designed, built, and is now operated by the Johns Hopkins Applied Physics Laboratory as part of NASA's Living with a Star (LWS) program (contract NNN06AA01C). This work was supported by the NASA Parker Solar Probe Program Office for the WISPR program (contract NNG11EK11I). Support from the LWS management and technical team has played a critical role in the success of the Parker Solar Probe mission. The FIELDS experiment on the Parker Solar Probe spacecraft was designed and developed under NASA contract NNN06AA01C.

Thanks to the Solar Wind Electrons, Alphas, and Protons (SWEAP) team for providing data (PI: Justin Kasper, BWX Technologies) also to the FIELDS team for providing data (PI: Stuart D. Bale, UC Berkeley). The Wide-Field Imager for Parker Solar Probe (WISPR) instrument was designed, built, and is now operated by the US Naval Research Laboratory in collaboration with Johns Hopkins University/Applied Physics Laboratory, California Institute of Technology/Jet Propulsion Laboratory, University of Gottingen, Germany, Centre Spatiale de Liege, Belgium and University of Toulouse/Research Institute in Astrophysics and Planetology. Solar Orbiter is a space mission of international collaboration between ESA and NASA, operated by ESA. The EUI instrument was built by CSL, IAS, MPS, MSSL/UCL, PMOD/WRC, ROB, LCF/IO with funding from the Belgian Federal Science Policy Office (BELSPO/PRODEX PEA 4000134088); the Centre National d'Etudes Spatiales (CNES); the UK Space Agency (UKSA); the Bundesministerium für Wirtschaft und Energie (BMWi) through the Deutsches Zentrum für Luft- und Raumfahrt (DLR); and the Swiss Space Office (SSO). The SoloHI instrument was designed and built at the U.S. Naval Research Laboratory and supported by NASA under contract NNG09EK11I. Metis was built and operated with funding from the Italian Space Agency (ASI), under contracts to the National Institute of Astrophysics (INAF) and industrial partners. Metis was built with hardware contributions from Germany (Bundesministerium für Wirtschaft und Energie through DLR), from the Czech Republic (PRODEX) and from ESA. The SECCHI data are produced by an international consortium of the NRL, LMSAL, and NASA GSFC (USA), RAL and U. Bham (UK), MPS (Germany), CSL (Belgium), IOTA, and IAS (France). The HMI data used are courtesy of NASA/SDO and the HMI science team. Partial funding for this project was supplied by the NASA HSO Connect Program, grant number 80NSSC20K1283, to the Smithsonian Astrophysical Observatory. MS and TN were supported by the Parker Solar Probe project through the SAO/SWEAP subcontract 975569. PH also acknowledges the support of the Office of Naval Research. PR gratefully acknowledges support from NASA (80NSSC20K0695, 80NSSC20C0187, 80NSSC20K1403, and 80NSSC22CA210).

## Conflict of interest

PR is employed by Predictive Science Inc.

The remaining authors declare that the research was conducted in the absence of any commercial or financial relationships that could be construed as a potential conflict of interest.

## Publisher's note

All claims expressed in this article are solely those of the authors and do not necessarily represent those of their affiliated organizations, or those of the publisher, the editors, and the reviewers. Any product that may be evaluated in this article, or claim that may be made by its manufacturer, is not guaranteed or endorsed by the publisher.

## References

Alterman, B. L., Kasper, J. C., Stevens, M. L., and Koval, A. (2018). A comparison of alpha particle and proton beam differential flows in collisionally young solar wind. *ApJ* 864, 112. doi:10.3847/1538-4357/aad23f

Andretta, V., Bemporad, A., De Leo, Y., Jerse, G., Landini, F., Mierla, M., et al. (2021). The first coronal mass ejection observed in both visible-light and UV H I Ly-$\alpha$ channels of the Metis coronagraph on board Solar Orbiter. *AAP* 656, L14. doi:10.1051/0004-6361/202142407

Antonucci, E., Romoli, M., Andretta, V., Fineschi, S., Heinzel, P., Moses, J. D., et al. (2020). Metis: The solar orbiter visible light and ultraviolet coronal imager. *AAP* 642, A10. doi:10.1051/0004-6361/201935338

Bale, S. D., Goetz, K., Harvey, P. R., Turin, P., Bonnell, J. W., Dudok de Wit, T., et al. (2016). The FIELDS instrument suite for solar Probe plus. Measuring the coronal plasma and magnetic field, plasma waves and turbulence, and radio signatures of solar transients. *SSR* 204, 49–82. doi:10.1007/s11214-016-0244-5

Biondo, R., Bemporad, A., Mignone, A., and Reale, F. (2021). Reconstruction of the parker spiral with the reverse *in situ* data and MHD APproach - rimap. *J. Space Weather Space Clim.* 11, 7. doi:10.1051/swsc/2020072

Borovsky, J. E. (2008). Flux tube texture of the solar wind: Strands of the magnetic carpet at 1 AU? *J. Geophys. Res. (Space Phys.* 113, A08110. doi:10.1029/2007JA012684

Borrini, G., Gosling, J. T., Bame, S. J., and Feldman, W. C. (1982). Helium abundance enhancements in the solar wind. *JGR* 87, 7370–7378. doi:10.1029/JA087iA09p07370

Bothmer, V., and Schwenn, R. (1994). Eruptive prominences as sources of magnetic clouds in the solar wind. *SSR* 70, 215–220. doi:10.1007/BF00777872

Braga, C. R., Vourlidas, A., Liewer, P. C., Hess, P., Stenborg, G., and Riley, P. (2022). Coronal Mass Ejection Deformation at 0.1 au Observed by WISPR. *ApJ* 938, 13. doi:10.3847/1538-4357/ac90bf

Brueckner, G. E., Howard, R. A., Koomen, M. J., Korendyke, C. M., Michels, D. J., Moses, J. D., et al. (1995). The large angle spectroscopic coronagraph (LASCO). *Sol. Phys.* 162, 357–402. doi:10.1007/BF00733434

Burlaga, L., Fitzenreiter, R., Lepping, R., Ogilvie, K., Szabo, A., Lazarus, A., et al. (1998). A magnetic cloud containing prominence material: January 1997. *JGR* 103, 277–285. doi:10.1029/97JA02768

Burlaga, L. F., Klein, L., Sheeley, J., Michels, D. J., Howard, R. A., Koomen, M. J., et al. (1982). A magnetic cloud and a coronal mass ejection. *GRL* 9, 1317–1320. doi:10.1029/GL009i012p01317

Case, A. W., Kasper, J. C., Stevens, M. L., Korreck, K. E., Paulson, K., Daigneau, P., et al. (2020). The solar Probe cup on the parker solar Probe. *ApJS* 246, 43. doi:10.3847/1538-4365/ab5a7b

DeForest, C. E., Howard, T. A., and McComas, D. J. (2013). Tracking coronal features from the low corona to Earth: A quantitative analysis of the 2008 december 12 coronal mass ejection. *ApJ* 769, 43. doi:10.1088/0004-637X/769/1/43

Domingo, V., Fleck, B., and Poland, A. I. (1995). SOHO: The solar and heliospheric observatory. *SSR* 72, 81–84. doi:10.1007/BF00768758

Fox, N. J., Velli, M. C., Bale, S. D., Decker, R., Driesman, A., Howard, R. A., et al. (2016). The solar Probe plus mission: Humanity's first visit to our star. *SSR* 204, 7–48. doi:10.1007/s11214-015-0211-6

Freeland, S. L., and Handy, B. N. (1998). Data analysis with the SolarSoft system. *Sol. Phys.* 182, 497–500. doi:10.1023/A:1005038224881

Gibson, S. E. (2018). Solar prominences: Theory and models. Fleshing out the magnetic skeleton. *Living Rev. Sol. Phys.* 15, 7. doi:10.1007/s41116-018-0016-2

Gopalswamy, N., Shimojo, M., Lu, W., Yashiro, S., Shibasaki, K., and Howard, R. A. (2003). Prominence eruptions and coronal mass ejection: A statistical study using microwave observations. *ApJ* 586, 562–578. doi:10.1086/367614

Hess, P., Howard, R. A., Stenborg, G., Linton, M., Vourlidas, A., Thernisien, A., et al. (2021). In-flight calibration and data reduction for the WISPR instrument on board the PSP mission. *Sol. Phys.* 296, 94. doi:10.1007/s11207-021-01847-9

Hess, P., Rouillard, A. P., Kouloumvakos, A., Liewer, P. C., Zhang, J., Dhakal, S., et al. (2020). WISPR imaging of a pristine CME. *ApJS* 246, 25. doi:10.3847/1538-4365/ab4ff0

Hess, P., and Zhang, J. (2017). A study of the earth-affecting CMEs of solar cycle 24. *Sol. Phys.* 292, 80. doi:10.1007/s11207-017-1099-y

Hirshberg, J., Bame, S. J., and Robbins, D. E. (1972). Solar flares and solar wind helium enrichments: July 1965 July 1967. *SolPhys* 23, 467–486. doi:10.1007/BF00148109

Horbury, T. S., O'Brien, H., Carrasco Blazquez, I., Bendyk, M., Brown, P., Hudson, R., et al. (2020). The solar orbiter magnetometer. *AAP* 642, A9. doi:10.1051/0004-6361/201937257

Howard, R. A., Moses, J. D., Vourlidas, A., Newmark, J. S., Socker, D. G., Plunkett, S. P., et al. (2008). Sun Earth connection coronal and heliospheric investigation (SECCHI). *SSR* 136, 67–115. doi:10.1007/s11214-008-9341-4

Howard, R. A., Stenborg, G., Vourlidas, A., Gallagher, B. M., Linton, M. G., Hess, P., et al. (2022). Overview of the remote sensing observations from PSP solar encounter 10 with perihelion at 13.3 $R_{\odot}$. *ApJ* 936, 43. doi:10.3847/1538-4357/ac7ff5

Howard, R. A., Vourlidas, A., Colaninno, R. C., Korendyke, C. M., Plunkett, S. P., Carter, M. T., et al. (2020). The solar orbiter heliospheric imager (SoloHI). *AAP* 642, A13. doi:10.1051/0004-6361/201935202

Howard, T. A., and DeForest, C. E. (2012). Inner heliospheric flux rope evolution via imaging of coronal mass ejections. *ApJ* 746, 64. doi:10.1088/0004-637X/746/1/64

Inhester, B. (2006). *Stereoscopy basics for the STEREO mission*. arXiv e-prints , astro-ph/0612649.

Kaiser, M. L. (2005). The STEREO mission: An overview. *Adv. Space Res.* 36, 1483–1488. doi:10.1016/j.asr.2004.12.066

Kasper, J. C., Abiad, R., Austin, G., Balat-Pichelin, M., Bale, S. D., Belcher, J. W., et al. (2016). Solar wind electrons alphas and protons (SWEAP) investigation: Design of the solar wind and coronal plasma instrument suite for solar Probe plus. *SSR* 204, 131–186. doi:10.1007/s11214-015-0206-3

Kilpua, E. K. J., Good, S. W., Palmerio, E., Asvestari, E., Lumme, E., Ala-Lahti, M., et al. (2019). Multipoint observations of the june 2012 interacting interplanetary flux ropes. *Front. Astronomy Space Sci.* 6, 50. doi:10.3389/fspas.2019.00050

Landau, L. D., and Lifshitz, E. M. (1987). *Fluid mechanics*. Butterworth-Heinemann, Elsevier.

Lepri, S. T., and Rivera, Y. J. (2021). Elemental abundances of prominence material inside ICMEs. *ApJ* 912, 51. doi:10.3847/1538-4357/abea9f

Lionello, R., Linker, J. A., and Mikić, Z. (2001). Including the transition region in models of the large-scale solar corona. *ApJ* 546, 542–551. doi:10.1086/318254

Lionello, R., Linker, J. A., and Mikić, Z. (2009). Multispectral emission of the sun during the first whole sun month: Magnetohydrodynamic simulations. *ApJ* 690, 902–912. doi:10.1088/0004-637X/690/1/902

Livi, R., Larson, D. E., Kasper, J. C., Abiad, R., Case, A. W., Klein, K. G., et al. (2022). The solar Probe ANalyzer-ions on the parker solar Probe. *ApJ* 938, 138. doi:10.3847/1538-4357/ac93f5

Luhmann, J. G., Gopalswamy, N., Jian, L. K., and Lugaz, N. (2020). ICME evolution in the inner heliosphere. *Sol. Phys.* 295, 61. doi:10.1007/s11207-020-01624-0

MacQueen, R. M., Csoeke-Poeckh, A., Hildner, E., House, L., Reynolds, R., Stanger, A., et al. (1980). The high altitude observatory coronagraph/polarimeter on the solar maximum mission. *Sol. Phys.* 65, 91–107. doi:10.1007/BF00151386

MacQueen, R. M., Eddy, J. A., Gosling, J. T., Hildner, E., Munro, R. H., Newkirk, J., et al. (1974). The outer solar corona as observed from Skylab: Preliminary results. *ApJL* 187, L85. doi:10.1086/181402

Mampaey, B., Verbeeck, F., Stegen, K., Kraaikamp, E., Gissot, S., Auchère, F., et al. (2022). *Solo/eui data release 5.0 2022-04*. Published by Royal Observatory of Belgium (ROB). doi:10.24414/2qfw-tr95

Marsch, E., Schwenn, R., Rosenbauer, H., Muehlhaeuser, K. H., Pilipp, W., and Neubauer, F. M. (1982). Solar wind protons: Three-dimensional velocity distributions and derived plasma parameters measured between 0.3 and 1 AU. *JGR* 87, 52–72. doi:10.1029/JA087iA01p00052

Mierla, M., Seaton, D. B., Berghmans, D., Chifu, I., De Groof, A., Inhester, B., et al. (2013). Study of a prominence eruption using PROBA2/SWAP and STEREO/EUVI data. *Sol. Phys.* 286, 241–253. doi:10.1007/s11207-012-9965-0

Mignone, A., Bodo, G., Massaglia, S., Matsakos, T., Tesileanu, O., Zanni, C., et al. (2007). Pluto: A numerical code for computational Astrophysics. *ApJS* 170, 228–242. doi:10.1086/513316

Mignone, A., Zanni, C., Tzeferacos, P., van Straalen, B., Colella, P., and Bodo, G. (2012). The PLUTO code for adaptive mesh computations in astrophysical fluid dynamics. *ApJS* 198, 7. doi:10.1088/0067-0049/198/1/7

Müller, D., Cyr, St.O. C., Zouganelis, I., Gilbert, H. R., Marsden, R., Nieves-Chinchilla, T., et al. (2020). The Solar Orbiter mission. Science overview. *AAP* 642, A1. doi:10.1051/0004-6361/202038467

Munro, R. H., Gosling, J. T., Hildner, E., MacQueen, R. M., Poland, A. I., and Ross, C. L. (1979). The association of coronal mass ejection transients with other forms of solar activity. *Sol. Phys.* 61, 201–215. doi:10.1007/BF00155456

Ness, N. F., and Burlaga, L. F. (2001). Spacecraft studies of the interplanetary magnetic field. *JGR* 106, 15803–15817. doi:10.1029/2000JA000118

Nieves-Chinchilla, T., Alzate, N., Cremades, H., Rodríguez-García, L., Dos Santos, L. F. G., Narock, A., et al. (2022). Direct first parker solar Probe observation of the interaction of two successive interplanetary coronal mass ejections in 2020 november. *ApJ* 930, 88. doi:10.3847/1538-4357/ac590b

Odstrcil, D., and Pizzo, V. J. (2009). Numerical heliospheric simulations as assisting tool for interpretation of observations by STEREO heliospheric imagers. *Sol. Phys.* 259, 297–309. doi:10.1007/s11207-009-9449-z

Ogilvie, K. W., and Desch, M. D. (1997). The wind spacecraft and its early scientific results. *Adv. Space Res.* 20, 559–568. doi:10.1016/S0273-1177(97)00439-0

O'Hara, J. P., Mierla, M., Podladchikova, O., D'Huys, E., and West, M. J. (2019). Exceptional extended field-of-view observations by PROBA2/SWAP on 2017 April 1 and 3. *ApJ* 883, 59. doi:10.3847/1538-4357/ab3b08

Owen, C. J., Bruno, R., Livi, S., Louarn, P., Al Janabi, K., Allegrini, F., et al. (2020). The solar orbiter solar wind analyser (SWA) suite. *AAP* 642, A16. doi:10.1051/0004-6361/201937259

Palmerio, E., Nieves-Chinchilla, T., Kilpua, E. K. J., Barnes, D., Zhukov, A. N., Jian, L. K., et al. (2021). Magnetic structure and propagation of two interacting CMEs from the sun to saturn. *J. Geophys. Res. (Space Phys.* 126, e2021JA029770. doi:10.1029/2021JA029770

Parenti, S. (2014). Solar prominences: Observations. *Living Rev. Sol. Phys.* 11, 1. doi:10.12942/lrsp-2014-1

Parker, E. N. (1958). Dynamics of the interplanetary gas and magnetic fields. *ApJ* 128, 664. doi:10.1086/146579

Patel, R., Majumdar, S., Pant, V., and Banerjee, D. (2022). A simple radial gradient filter for batch-processing of coronagraph images. *Sol. Phys.* 297, 27. doi:10.1007/s11207-022-01957-y

Pesnell, W. D., Thompson, B. J., and Chamberlin, P. C. (2012). The solar dynamics observatory (SDO). *Sol. Phys.* 275, 3–15. doi:10.1007/s11207-011-9841-3

Pizzo, V. J. (1981). On the application of numerical models to the inverse mapping of solar wind flow structures. *JGR* 86, 6685–6690. doi:10.1029/JA086iA08p06685

Pomoell, J., and Poedts, S. (2018). Euhforia: European heliospheric forecasting information asset. *J. Space Weather Space Clim.* 8, A35. doi:10.1051/swsc/2018020

Priest, E. R., Hood, A. W., and Anzer, U. (1989). A twisted flux-tube model for solar prominences. I. General properties. *ApJ* 344, 1010. doi:10.1086/167868

Reeves, K. K., Linker, J. A., Mikić, Z., and Forbes, T. G. (2010). Current sheet energetics, flare emissions, and energy partition in a simulated solar eruption. *ApJ* 721, 1547–1558. doi:10.1088/0004-637X/721/2/1547

Reva, A. A., Ulyanov, A. S., and Kuzin, S. V. (2016). Current sheet structures observed by the TESIS EUV telescope during a flux rope eruption on the sun. *ApJ* 832, 16. doi:10.3847/0004-637X/832/1/16

Richardson, I. G., Cliver, E. W., and Cane, H. V. (2000). Sources of geomagnetic activity over the solar cycle: Relative importance of coronal mass ejections, high-speed streams, and slow solar wind. *JGR* 105, 18203, 203–18213, 213. doi:10.1029/1999JA000400

Riley, P., Linker, J. A., and Arge, C. N. (2015). On the role played by magnetic expansion factor in the prediction of solar wind speed. *Space weather.* 13, 154–169. doi:10.1002/2014SW001144

Riley, P., Linker, J. A., and Mikić, Z. (2001). An empirically-driven global MHD model of the solar corona and inner heliosphere. *JGR* 106, 15889–15901. doi:10.1029/2000JA000121

Riley, P., Lionello, R., Caplan, R. M., Downs, C., Linker, J. A., Badman, S. T., et al. (2021). Using Parker Solar Probe observations during the first four perihelia to constrain global magnetohydrodynamic models. *AAP* 650, A19. doi:10.1051/0004-6361/202039815

Rochus, P., Auchère, F., Berghmans, D., Harra, L., Schmutz, W., Schühle, U., et al. (2020). The solar orbiter EUI instrument: The extreme ultraviolet imager. *AAP* 642, A8. doi:10.1051/0004-6361/201936663

Rodriguez, L., Warmuth, A., Andretta, V., Mierla, M., Zhukov, A. N., Shukhobodskaia, D., et al. (2023). The eruption of 22 April 2021 as observed by solar orbiter: Continuous magnetic reconnection and heating after the impulsive phase. *SolPhys* 298, 1. doi:10.1007/s11207-022-02090-6

Romoli, M., Antonucci, E., Andretta, V., Capuano, G. E., Da Deppo, V., De Leo, Y., et al. (2021). First light observations of the solar wind in the outer corona with the Metis coronagraph. *AAP* 656, A32. doi:10.1051/0004-6361/202140980

Rouillard, A. P. (2011). Relating white light and *in situ* observations of coronal mass ejections: A review. *J. Atmos. Solar-Terrestrial Phys.* 73, 1201–1213. doi:10.1016/j.jastp.2010.08.015

Schatten, K. H. (1971). Current sheet magnetic model for the solar corona. *Cosm. Electrodyn.* 2, 232–245.

Schou, J., Scherrer, P. H., Bush, R. I., Wachter, R., Couvidat, S., Rabello-Soares, M. C., et al. (2012). Design and ground calibration of the helioseismic and magnetic imager (HMI) instrument on the solar dynamics observatory (SDO). *Sol. Phys.* 275, 229–259. doi:10.1007/s11207-011-9842-2

Scolini, C., Chané, E., Temmer, M., Kilpua, E. K. J., Dissauer, K., Veronig, A. M., et al. (2020). CME-CME interactions as sources of CME geoeffectiveness: The formation of the complex ejecta and intense geomagnetic storm in 2017 early september. *ApJS* 247, 21. doi:10.3847/1538-4365/ab6216

Seaton, D. B., Hughes, J. M., Tadikonda, S. K., Caspi, A., DeForest, C. E., Krimchansky, A., et al. (2021). The Sun's dynamic extended corona observed in extreme ultraviolet. *Nat. Astron.* 5, 1029–1035. doi:10.1038/s41550-021-01427-8

Sheeley, J., Michels, D. J., Howard, R. A., and Koomen, M. J. (1980). Initial observations with the SOLWIND coronagraph. *ApJL* 237, L99–L101. doi:10.1086/183243

Shi, C., Velli, M., Bale, S. D., Réville, V., Maksimović, M., and Dakeyo, J.-B. (2022). Acceleration of polytropic solar wind: Parker Solar Probe observation and one-dimensional model. *Phys. Plasmas* 29, 122901. doi:10.1063/5.0124703

Stone, E. C., Frandsen, A. M., Mewaldt, R. A., Christian, E. R., Margolies, D., Ormes, J. F., et al. (1998). The advanced composition explorer. *SSR* 86, 1–22. doi:10.1023/A:1005082526237

Tasnim, S., Cairns, I. H., and Wheatland, M. S. (2018). A generalized equatorial model for the accelerating solar wind. *J. Geophys. Res. (Space Phys.* 123, 1061–1085. doi:10.1002/2017JA024532

Thernisien, A. F. R., Howard, R. A., and Vourlidas, A. (2006). Modeling of flux rope coronal mass ejections. *ApJ* 652, 763–773. doi:10.1086/508254

Thernisien, A., Vourlidas, A., and Howard, R. A. (2009). Forward modeling of coronal mass ejections using STEREO/SECCHI data. *Sol. Phys.* 256, 111–130. doi:10.1007/s11207-009-9346-5

Tousey, R., Bartoe, J. D. F., Bohlin, J. D., Brueckner, G. E., Purcell, J. D., Scherrer, V. E., et al. (1973). A preliminary study of the extreme ultraviolet spectroheliograms from Skylab. *Sol. Phys.* 33, 265–280. doi:10.1007/BF00152418

Velli, M., Harra, L. K., Vourlidas, A., Schwadron, N., Panasenco, O., Liewer, P. C., et al. (2020). Understanding the origins of the heliosphere: Integrating observations and measurements from parker solar Probe, solar orbiter, and other space- and ground-based observatories. *AAP* 642, A4. doi:10.1051/0004-6361/202038245

Vourlidas, A., Howard, R. A., Plunkett, S. P., Korendyke, C. M., Thernisien, A. F. R., Wang, D., et al. (2016). The wide-field imager for solar Probe plus (WISPR). *SSR* 204, 83–130. doi:10.1007/s11214-014-0114-y

Wang, J., Feng, H., and Zhao, G. (2018). Cold prominence materials detected within magnetic clouds during 1998-2007. *AAP* 616, A41. doi:10.1051/0004-6361/201731807

Webb, D. F., and Howard, T. A. (2012). Coronal mass ejections: Observations. *Living Rev. Sol. Phys.* 9, 3. doi:10.12942/lrsp-2012-3

Weber, E. J., and Davis, J. (1967). The angular momentum of the solar wind. *ApJ* 148, 217–227. doi:10.1086/149138

Whittlesey, P. L., Larson, D. E., Kasper, J. C., Halekas, J., Abatcha, M., Abiad, R., et al. (2020). The solar Probe ANalyzers—electrons on the parker solar Probe. *ApJS* 246, 74. doi:10.3847/1538-4365/ab7370

Wood, B. E., Hess, P., Howard, R. A., Stenborg, G., and Wang, Y.-M. (2020). Morphological reconstruction of a small transient observed by parker solar Probe on 2018 november 5. *ApJS* 246, 28. doi:10.3847/1538-4365/ab5219

Wood, B. E., Wu, C.-C., Lepping, R. P., Nieves-Chinchilla, T., Howard, R. A., Linton, M. G., et al. (2017). A STEREO survey of magnetic cloud coronal mass ejections observed at Earth in 2008-2012. *ApJS* 229, 29. doi:10.3847/1538-4365/229/2/29

Yermolaev, Y. I., Lodkina, I. G., Yermolaev, M. Y., Riazantseva, M. O., Rakhmanova, L. S., Borodkova, N. L., et al. (2020). Dynamics of large-scale solar-wind streams obtained by the double superposed epoch analysis: 4. Helium abundance. *J. Geophys. Res. (Space Phys.* 125, e27878. doi:10.1029/2020JA027878

Zhao, X., Liu, Y. D., Hu, H., and Wang, R. (2019). Quantifying the propagation of fast coronal mass ejections from the sun to interplanetary space by combining remote sensing and multi-point *in situ* observations. *ApJ* 882, 122. doi:10.3847/1538-4357/ab379b

Zurbuchen, T. H., and Richardson, I. G. (2006). *In-situ* solar wind and magnetic field signatures of interplanetary coronal mass ejections. *SSR* 123, 31–43. doi:10.1007/s11214-006-9010-4

Zurbuchen, T. H., Weberg, M., von Steiger, R., Mewaldt, R. A., Lepri, S. T., and Antiochos, S. K. (2016). Composition of coronal mass ejections. *ApJ* 826, 10. doi:10.3847/0004-637X/826/1/10